OPTICS

10.1126/sciadv.1501489

A broadband chip-scale optical frequency synthesizer at 2.7×10^{-16} relative uncertainty

Shu-Wei Huang,[1]* Jinghui Yang,[1] Mingbin Yu,[2] Bart H. McGuyer,[3] Dim-Lee Kwong,[2] Tanya Zelevinsky,[3] Chee Wei Wong[1]*

Optical frequency combs—coherent light sources that connect optical frequencies with microwave oscillations—have become the enabling tool for precision spectroscopy, optical clockwork, and attosecond physics over the past decades. Current benchmark systems are self-referenced femtosecond mode-locked lasers, but Kerr nonlinear dynamics in high-*Q* solid-state microresonators has recently demonstrated promising features as alternative platforms. The advance not only fosters studies of chip-scale frequency metrology but also extends the realm of optical frequency combs. We report the full stabilization of chip-scale optical frequency combs. The microcomb's two degrees of freedom, one of the comb lines and the native 18-GHz comb spacing, are simultaneously phase-locked to known optical and microwave references. Active comb spacing stabilization improves long-term stability by six orders of magnitude, reaching a record instrument-limited residual instability of 3.6 mHz/$\sqrt{\tau}$. Comparing 46 nitride frequency comb lines with a fiber laser frequency comb, we demonstrate the unprecedented microcomb tooth-to-tooth relative frequency uncertainty down to 50 mHz and 2.7×10^{-16}, heralding novel solid-state applications in precision spectroscopy, coherent communications, and astronomical spectrography.

INTRODUCTION

High-*Q* microresonators (*1*), by efficiently trapping photons in wavelength-scale structures for as long as microseconds, greatly enhance the light-matter interaction and enable novel studies in a wide range of fields, including cavity quantum electrodynamics (*2*), parity-time symmetry breaking (*3*), single-molecule detection (*4*), and dynamical nonlinear science (*5*, *6*). Moreover, continuous-wave–pumped high-*Q* microresonators have recently emerged as promising alternative platforms for ultrashort pulse and optical frequency comb generation (*7*–*11*). Comb spacing uniformity of microresonator-based optical frequency combs, or Kerr microcombs, has been studied either by comparison with a fiber laser frequency comb (FFC) (*12*) or by parametric comb folding technique (*13*). Full comb stabilization has been demonstrated in a silica microtoroid with a free spectral range of 86 GHz (*14*), and *f-2f* or *2f-3f* comb self-referencing techniques have been applied to these whispering gallery mode (WGM) microresonators (*15*). Kerr microcombs are unique in their compact footprints and suitably large comb spacings, thereby expanding the already remarkable applications of frequency comb metrology. Microresonators with microwave free spectral ranges have recently been advanced in both WGM structures (*16*–*19*) and planar ring geometries (*20*–*22*). Although complementary metal-oxide semiconductor (CMOS)–compatible ring resonators are particularly attractive because of their monolithic electronic and photonic integration capabilities, to date, there has been no demonstration of the full stabilization of these chip-scale planar microresonators.

Here, we report the first fully stabilized CMOS-compatible chip-scale Kerr microcomb with a frequency relative uncertainty of 2.7×10^{-16}. The silicon nitride spiral resonator is designed and fabricated to generate a Kerr microcomb, at 18-GHz native spacing and spanning more than 8 THz over more than 400 comb lines. The comb's two degrees of freedom, one of the comb line frequencies and the comb spacing, are phase-locked to a known optical reference and a microwave synthesizer, respectively. Active stabilization on the comb spacing improves the radio-frequency (RF) stability by six orders of magnitude, reaching a residual instrument-limited close-to-carrier (10 Hz) phase noise of −70 dBc/Hz and an Allan deviation of 3.6 mHz/$\sqrt{\tau}$. In the optical frequency, 46 lines of the Kerr microcomb subset are selected and compared against the current benchmark FFC, and the frequency relative uncertainty of the stabilized Kerr microcomb is demonstrated down to 50 mHz. The reported system is a promising compact platform for coherent Raman spectroscopy (*23*), optical clockwork (*24*, *25*), coherent communications (*26*), arbitrary waveform generation (*27*), and astrophysical spectrography (*28*–*30*).

RESULTS

Figure 1A shows the experimental setup for the generation and stabilization of the Kerr microcomb. The silicon nitride spiral resonator is fabricated with CMOS-compatible processes, and the waveguide cross section is designed to have small and flattened group velocity dispersion for broadband comb generation. Planar ring geometry is used because of the reduced sensitivity to environmental perturbation, along with the fewer discrete transverse resonator modes, and the flexibility to tailor the cavity dispersion for efficient and broadband comb generation. Properties of the Si_3N_4 microresonator are detailed in section SI. The loaded quality factor *Q* of the pump mode is 660,000 (intrinsic *Q*, ~1,300,000), and 1 W of pump power is critically coupled to the microresonator, resulting in a maximum coupled pump power five times higher than the threshold pump power. The output is first shortpass-filtered using a 1550/1590-nm wavelength division multiplexer and then boosted in power with a 13-dBm C-band preamplifier to increase the signal-to-noise ratio (SNR) of the photodetector signal. Figure 1B shows the Kerr microcomb spectrum, spanning more than 8 THz and consisting of more than 400 comb lines. To ensure that the Kerr microcomb is

[1]Mesoscopic Optics and Quantum Electronics Laboratory, University of California, Los Angeles, CA 90095, USA. [2]Institute of Microelectronics, Agency for Science, Technology and Research (A*STAR), Singapore 117865, Singapore. [3]Department of Physics, Columbia University, New York, NY 10027, USA.
*Corresponding author. E-mail: swhuang@seas.ucla.edu (S.-W.H.); cheewei.wong@ucla.edu (C.W.W.)

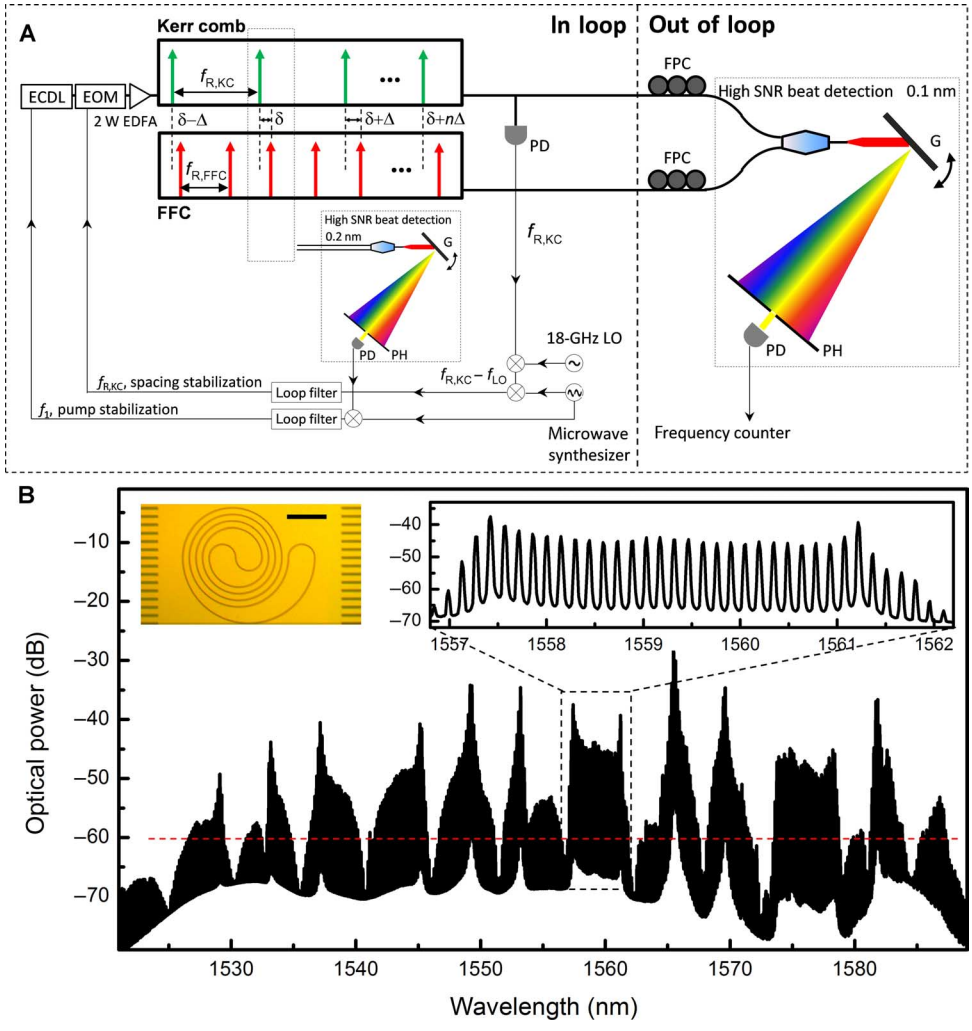

Fig. 1. A stabilized chip-scale optical frequency comb. (**A**) Measurement setup schematic for the generation and stabilization of the chip-scale optical frequency comb. To stabilize the comb's first degree of freedom, we phase-locked the ECDL to an optical reference (here a mode of a stabilized FFC) and then amplified it to 2 W to pump the Si_3N_4 microresonator. To stabilize the comb's second degree of freedom, we monitored the Kerr comb spacing $f_{R,KC}$ by sending the comb to a high-speed photodetector (more than 15 GHz with a 3-dB bandwidth) and downmixing the electronic signal to the baseband with a local oscillator at f_{LO} = 18 GHz. A fiber electro-optic modulator (EOM) controls the pump power and stabilizes the comb spacing. $\Delta = f_{R,KC} - [f_{R,KC}/f_{R,FFC}]f_{R,FFC}$. δ, Frequency difference between the pump and the adjacent FFC line; PD, photodetector; G, grating; PH, pinhole; FPC, fiber polarization controller. (**B**) Example of a stabilized Kerr frequency comb spectrum, consisting of more than 400 comb lines in the telecommunication wavelength range. The horizontal (red) dashed line denotes a power level of 1 μW per comb line. Left inset: Optical micrograph of the spiral microresonator. Scale bar, 250 μm. Right inset: Clearly observed comb lines with native spacing at the cavity's free spectral range.

driven from a noisy state to a phase-locked state (*22*) and to verify that it does not consist of many sub-comb families with offsets (*31*, *32*), we monitored RF amplitude noise and the fundamental beat note of different filtered Kerr microcomb segments, with details shown in sections SII and SIII.

For stabilization of the Kerr microcomb, one of the comb lines and the comb spacing are phase-locked to a known optical reference and a microwave synthesizer, respectively. In our system, the known optical reference is derived from an approximately 200-Hz stabilized erbium FFC (Menlo Systems), which is also used as a calibration standard to assess the uncertainty of the Kerr microcomb. A rubidium-locked diode laser can also be used as the optical reference (*33*, *34*), with details presented in section SV. In Fig. 1A, 1% of the pump mode, which is also the strongest Kerr microcomb line, is tapped and beat with the optical reference on a photodetector. To ensure that the beat note has sufficient SNR for reliable feedback stabilization [more than 35 dB with a 100-kHz resolution bandwidth (RBW)], we built a 0.2-nm narrow-bandwidth monochromator to filter the FFC before it is beat with the pump. Figure 2A is the free-running beat note, showing a few megahertz of pump frequency drift in 1 s. For high-bandwidth control of the pump frequency, the diode current of the external-cavity diode laser (ECDL) is directly modulated. However, such high-bandwidth feedback control has a trade-off—amplitude modulation of the pump power and, consequently, excess instability in the comb spacing. Figure S4B depicts the dependence of comb spacing on pump power. This effect is partly compensated for by saturating the erbium-doped fiber amplifier

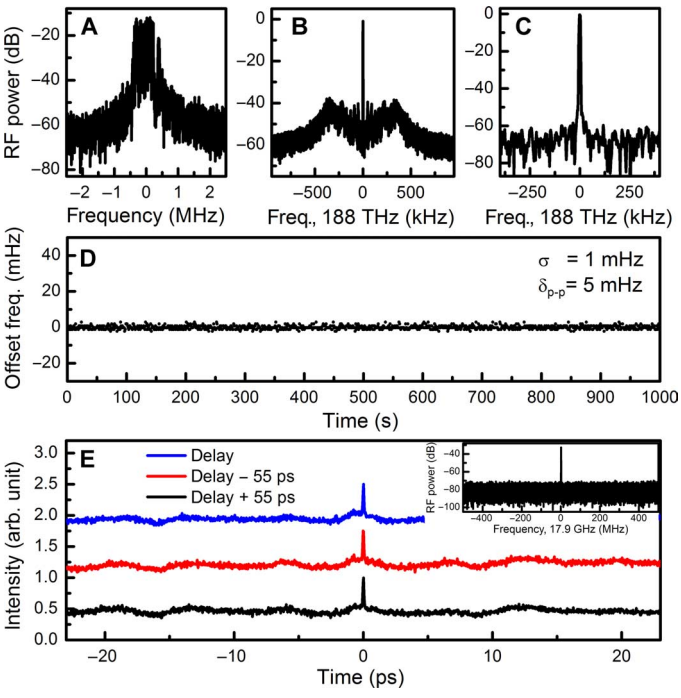

Fig. 2. Stabilizing the pump frequency to the millihertz-level residual error and time-domain picture of the phase-locked Kerr comb. (**A**) Free-running beat note between the pump and the FFC. To obtain a sufficient SNR for reliable feedback stabilization (more than 35 dB with a 100-kHz RBW), we built a 200-pm bandwidth monochromator to filter the FFC before it was mixed with the pump. Sweep time is 10 ms. (**B**) RF spectrum of the stabilized beat note with a 1-kHz RBW. Control of the pump frequency was achieved by modulating the ECDL diode current with a 300-kHz bandwidth. (**C**) RF spectrum of the stabilized beat note with a 6-Hz RBW, showing a resolution-limited linewidth of 6 Hz. (**D**) Frequency counting of the stabilized beat note with a gate time of 1 s. The SD over 1000 s is 1 mHz, instrument-limited by the stability of the frequency counter. (**E**) Optical intensity autocorrelations of the phase-locked Kerr frequency comb at different delays, evidently showing the repetitive structures and excluding the possibility of noise correlation. Inset: RF spectrum of the free-running comb spacing with a scan range much larger than the cavity linewidth (290 MHz). The comb was tuned to enter the phase-locked state by fine control of the pump frequency.

(EDFA) and later eliminated by the second feedback loop on the comb spacing. Figure 2B shows the stabilized beat note, illustrating a clear single peak at the center with uncompensated noise above the feedback bandwidth of 300 kHz. The beat has a 70-MHz offset to allow RF amplification for higher SNR in the feedback loop. Figure 2C is the zoom-in view of the stabilized beat note, showing a resolution-limited linewidth of 6 Hz. To quantify the long-term stability of the locked pump frequency, we analyzed the beat signal using a frequency counter and present the counting results in Fig. 2D. The pump frequency remains steady over 1000 s with an SD of 1 mHz and a peak-to-peak deviation of 5 mHz.

The comb spacing of 17.9 GHz is directly measurable by sending the output to a high-speed photodetector (more than 15 GHz with a 3-dB bandwidth). An 18-GHz local oscillator is used to downmix the electronic signal to the baseband for analysis. The inset to Fig. 2E plots the free-running comb spacing beat with a scan range of 1 GHz, showing a clean single peak characteristic of an equidistant Kerr microcomb. Details confirming the continuous equidistance of the Kerr microcomb are summarized in sections SII and SIII. Figure 2E illustrates the noncolinear second-harmonic-generation optical intensity autocorrelation to reveal the time-domain picture of the Kerr microcomb. Careful checks are done to make sure no colinear second-harmonic background is collected in the setup. Although the Kerr microcomb is operated in a low-noise state, clean circulating mode-locked pulses (*9*) are not formed, as evidenced by the elevated autocorrelation background of nearly half of the peak. Furthermore, the autocorrelation measurements are performed at three different delays, evidently showing the repetitive temporal structures of the Kerr microcomb and excluding the possibility of noise correlation. Here, a fixed phase relationship between different comb lines is obtained, but the phase relationship may contain some abrupt changes associated with the local dispersion disruptions. Thus, mode-locking is prohibited and δ-Δ matching becomes the underlying mechanism that drives the Kerr microcomb into a low-noise state (*16*, *19*, *31*, *32*).

The comb spacing is then phase-locked and stabilized to a microwave synthesizer by controlling the pump power with a fiber EOM. Pump power is an effective way to control the comb spacing through thermal expansion and thermo-optic effects (*35*) and nonlinear phase accumulation. Figure 3A shows the stabilized beat note, with a resolution-limited linewidth of 6 Hz and a low close-to-carrier phase noise. To characterize the frequency stability of the comb spacing, we measured the single sideband (SSB) phase noise spectra and Allan deviations and present the data in Fig. 3B. Free running with none of the feedback loops engaged, the phase noise of the comb spacing shows a $f^{-3.5}$ dependence on the offset frequency in the vicinity of the carrier. Such close-to-carrier behavior suggests that the phase noise is now dominated by a mixture of technical noise of frequency flicker (30 dB/decade) and frequency random walk (40 dB/decade), rather than limited by quantum noise phase diffusion (*36*). Because the microresonator is not thermally insulated from the environment, its interaction with the fluctuating ambient temperature results in the random walk of the comb spacing. Meanwhile, the pump wavelength drift leads to the flicker noise mediated by the residual optical absorption in the microresonator (*22*). However, such technical noise can be removed by phase-locking the beat note to a high-performance microwave synthesizer. As shown in Fig. 3B, the resulting close-to-carrier phase noise can reach the level of −70 dBc/Hz at 10 Hz with a $f^{-1.5}$ dependence on the offset frequency, limited only by the noise of the microwave synthesizer.

DISCUSSION

For offset frequency above 10 kHz, the phase noise of the fully stabilized comb spacing is better than that of the 18-GHz local oscillator used for downmixing the electronic signal. The measurement is instrument-limited to the level of ≥−108 dBc/Hz from 10 to 300 kHz and to the level of −130 dBc/Hz at 1 MHz. It is therefore informative to calculate the theoretical limit of the phase noise at large offset frequencies and compare it with the measurement. Using the equations with the pump-resonance detuning of $\frac{T_R\gamma^2}{D}$ derived from the study by Matsko and Maleki (*36*) and assuming $\left(\frac{f}{\gamma}\right)^2 \ll 1$, we obtain the lower limit of the phase noise expressed as

$$\mathcal{L}(f) \approx \frac{2\sqrt{2}\pi\hbar c n_2}{n_0^2 V_0} Q^2 \left[\frac{23}{24} + \left(\frac{4+\pi^2}{96\pi^2}\right)\frac{\gamma^2}{f^2}\right] \quad (1)$$

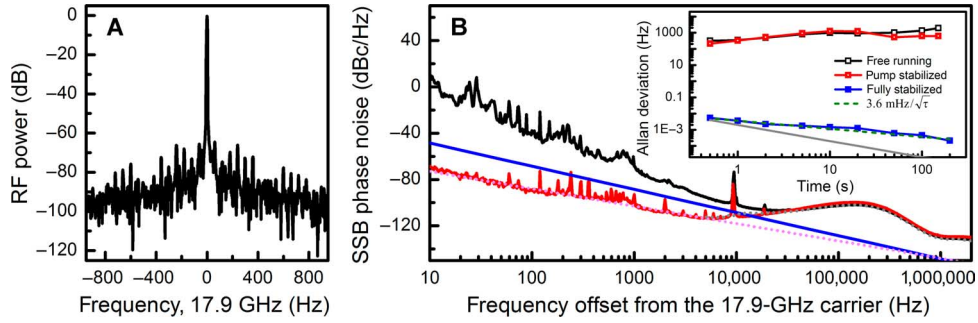

Fig. 3. Stabilizing the comb spacing to the millihertz-level residual error. (**A**) RF spectrum of the stabilized comb spacing, showing a resolution-limited linewidth of 6 Hz. Control of the comb spacing was achieved by modulating the pump power via a fiber EOM. (**B**) SSB phase noise of the free-running (black curve) and stabilized (red curve) comb spacing. Free running, the phase noise of the comb spacing shows a $f^{-3.5}$ dependence on the offset frequency in the vicinity of the carrier. Such technical noise can be removed by phase-locking the beat note to a high-performance microwave synthesizer, and the resulting close-to-carrier phase noise can reach the level of −70 dBc/Hz at 10 Hz with a $f^{-1.5}$ dependence on the offset frequency (pink dashed curve), limited only by the microwave synthesizer. On the other hand, for offset frequencies above 10 kHz, the phase noise of the comb spacing is better than that of the 18-GHz local oscillator used for downmixing the electronic signal (gray dashed curve), and the measurement is thus instrument-limited. The phase noise estimated from Eq. 1 is −148 dBc/Hz at 1 MHz, and it grows with a f^{-2} dependence on the offset frequency. The estimated phase noise reaches −108 dBc/Hz at 10 kHz and starts to exceed the noise level of the 18-GHz local oscillator, matching the experimental observations (blue curve). Inset: Allan deviation of the comb spacing under free running (black empty squares), pump frequency stabilization (red semifilled squares), and full stabilization (blue filled squares). The fully stabilized comb spacing shows a consistent trend of 3.6 mHz/$\sqrt{\tau}$ (green dashed line) when the gate time is in the range from 0.5 to 200 s. The gray line denotes the counterlimited Allan deviation.

where $D \equiv (\omega_{m+1} - \omega_m) - (\omega_m - \omega_{m-1})$, Q, n_0, n_2, V_0, 2γ, and f are the nonequidistance of the cold cavity modes, quality factor, linear refractive index, nonlinear refractive index, mode volume, full width at half maximum resonance linewidth, and frequency offset from the 17.9-GHz carrier, respectively. For our spiral microresonator, the estimated phase noise at 1 MHz is −148 dBc/Hz, and it grows quadratically with the inverse of the offset frequency. The estimated phase noise reaches −108 dBc/Hz at 10 kHz and starts to exceed the noise level of the 18-GHz local oscillator, matching the experimental observations. Notably, Eq. 1 derivation requires a single-mode microresonator and the Kerr microcomb to be mode-locked and hence only serves as a lower limit to our measurements.

The inset to Fig. 3B plots the Allan deviations of the comb spacing under different conditions. After the comb spacing is downmixed with the 18-GHz local oscillator, the beat frequency is counted with a Λ-type frequency counter. Allan deviation is then estimated using the equation $\sigma_A(\tau) = \sqrt{\frac{1}{M}\sum_{i=1}^{i=M}\frac{(\bar{y}_{i+1} - \bar{y}_i)^2}{2}}$, where $\tau, \bar{y}_i$, and $M = \min\{60, [\frac{1000}{\tau}]\}$ are the gate time, the fractional frequency, and the number of samples, respectively (*37*). Free running, the Allan deviation increases as $\tau^{1/3}$ as a result of technical noise, including the pump wavelength drift and the fluctuating ambient temperature (black empty squares). Pump frequency stabilization reduces the increase in Allan deviation over the gate time, but the level of Allan deviation remains unimproved because of the additional pump power fluctuation from the used pump frequency control (red semifilled squares). With pump power feedback control, the active stabilization on the comb spacing improves long-term stability by six orders of magnitude, reaching 3.6 mHz/$\sqrt{\tau}$ (blue filled squares). The residual comb instability is limited by the microwave synthesizer and comes close to the counter limit at a 1-s gate time.

To assess the uncertainty of the fully stabilized Kerr microcomb, we used the Menlo Systems FFC as the calibration standard and measured the out-of-loop frequencies of 46 Kerr microcomb lines around 1576 nm (Fig. 4A) by beating each comb line with the adjacent FFC mode, as shown in Fig. 1A. When the comb spacings of the FFC and Kerr microcomb are made unequal, the beat frequencies should strictly follow the relationship of

$$f_{\text{beat}}^{n} = \delta + n\left(f_{\text{R,KC}} - \left[\frac{f_{\text{R,KC}}}{f_{\text{R,FFC}}}\right] f_{\text{R,FFC}}\right) \quad (2)$$

where δ is the beat frequency at the pump mode, $f_{\text{R,KC}}$ is the Kerr microcomb spacing, and $f_{\text{R,FFC}}$ is the FFC spacing. Deviation from this expression poses an upper bound on the frequency uncertainty of the Kerr microcomb. Figure 4B shows two sample histograms of the frequency counting measurement. Six hundred counts are accumulated at the 1-s gate time for statistical analysis, and the Gaussian curve fitting is implemented to derive the mean values and SDs. Counting results on all 46 comb lines are shown in Fig. 4C. The mean values of the comb frequencies stray from the ideal with a 190-mHz peak-to-peak deviation and a 50-mHz SD. The relative frequency uncertainty of the stabilized chip-scale frequency comb is thus calculated as 2.7×10^{-16}, referenced to the optical carrier at 188 THz. Notably, the 17.9-GHz comb spacing generated directly from the microresonator is compatible with high-resolution astrospectroscopy; thus, sophisticated Fabry-Perot (FP) filtering cavities, which limit the precision of state-of-the-art astrocomb (*28*–*30*), are circumvented. Because of the residual FP cavity dispersion and fluctuations of the FP cavity resonance, leading to changes in the extraneous-line suppression, the uncertainty of the astrocomb line frequency is typically degraded to the kilohertz level (*28*–*30*). The uncertainty σ then translates linearly into the systematic error ε in astrophysical velocity measurements with an approximate relation of $\varepsilon \cong \frac{\sigma}{f_p} c$ (*28*). Thus, the 50-mHz frequency uncertainty of the Kerr microcomb can potentially improve the precision in astrophysical radial velocity measurements by orders of magnitude.

In summary, we report the first fully stabilized CMOS-compatible solid-state optical frequency comb. On the basis of the silicon nitride spiral resonator, a native 18-GHz Kerr microcomb is generated, and its

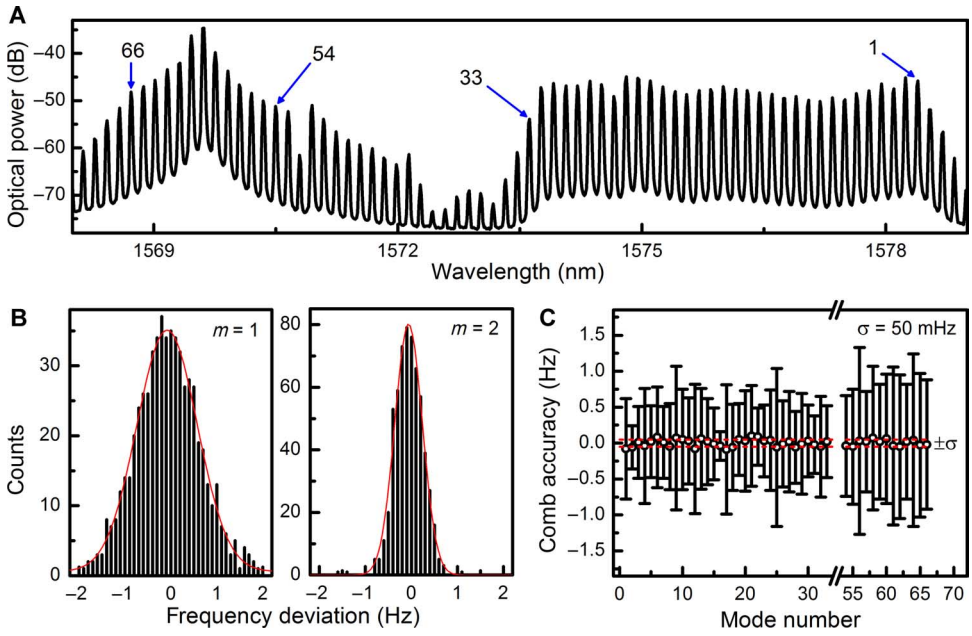

Fig. 4. Out-of-loop characterization of the fully stabilized chip-scale optical frequency comb. (**A**) To quantify the uncertainty of the stabilized chip-scale optical frequency comb, we mixed each of the comb lines from 1578.4 to 1573.6 nm ($m = 1$ to $m = 33$) and from 1570.5 to 1568.7 nm ($m = 54$ to $m = 66$) with the FFC and counted the beat frequency with a gate time of 1 s. The beat frequencies should change progressively by Δ, where $\Delta = f_{R,KC} - [f_{R,KC}/f_{R,FFC}]f_{R,FFC}$, and the deviation from this relationship poses an upper bound on the frequency uncertainty of the chip-scale optical frequency comb. (**B**) Sample histograms of the frequency counting measurement on the first and second modes (m). Six hundred counts are accumulated for statistical analysis. The red lines are the Gaussian fits to the histograms. (**C**) Counting results on the optical frequencies of 46 comb lines. The centroid of the comb frequencies strays from the ideal with a 190-mHz peak-to-peak deviation and a 50-mHz SD. The frequency relative uncertainty of the fully stabilized chip-scale optical frequency comb is thus calculated at 2.7×10^{-16}, referenced to the 188-THz optical carrier.

SSB phase noise reaches the instrument-limited floor of −130 dBc/Hz at 1-MHz offset. The comb's two degrees of freedom, one of the comb line frequencies and the comb spacing, are phase-locked to a known optical reference and a microwave synthesizer, respectively, reaching an instrument-limited residual comb spacing instability of $3.6\ \text{mHz}/\sqrt{\tau}$. Forty-six Kerr microcomb lines are compared with the current benchmark FFC, and the relative frequency uncertainty of the fully stabilized Kerr microcomb is measured down to 2.7×10^{-16}. The reported system is a promising scalable platform for coherent Raman spectroscopy, high-precision optical clockwork, high-capacity coherent communications, arbitrary waveform generation, and astrophysical spectrography.

MATERIALS AND METHODS

Microresonator characteristics

The silicon nitride waveguide cross section was designed to be 2 μm × 0.75 μm so that not only the group velocity dispersion but also the third-order dispersion was small at the pump wavelength. The spiral design ensured that the total footprint of the relatively large resonator could be minimized (less than $0.9 \times 0.8\ \text{mm}^2$), eliminating the additional cavity losses associated with the photomask stitching and discretization errors. The intrinsic quality factor of the spiral resonator was estimated to be 1,300,000. Bends in the resonator have diameters greater than 160 μm to minimize the bending-induced dispersion. Adiabatic mode converters were implemented on the side of the chip to improve the coupling efficiency from the free space to the bus waveguide, to less than a 3-dB coupling loss per facet. The gap between the bus waveguide and the microresonator was 500 nm, leading to a critical coupling at the pump wavelength.

Kerr comb generation

A tunable ECDL (Newfocus TLB-6730) was amplified by an L-band EDFA to 2 W and then coupled to the microresonator. The pump wavelength was 1598.7 nm. A 1583-nm longpass filter removed the amplified spontaneous emission noise from the EDFA. The microresonator chip temperature was actively stabilized to ±10 mK. A three-paddle fiber polarization controller and a polarization beam splitter cube were used to ensure proper coupling of the transverse-electric polarization into the microresonator. To obtain the Kerr microcomb, we first tuned the pump wavelength into the resonance from the high-frequency side at a step of 10 pm until primary comb lines were observed on the optical spectrum analyzer, before fine control, to drive the comb from a noisy state to a phase-locked state. The threshold pump power was estimated to be 200 mW using the equation $P_{\text{th}} = \frac{\pi}{8\eta}\frac{n_0}{n_2}\frac{\omega_P}{\omega_{FSR}}\frac{A}{Q^2}$, where $A = 1.3\ \mu\text{m}^2$ is the mode area, $\eta = 0.5$ is the coupling parameter, ω_P is the pump frequency, and ω_{FSR} is the cavity's free spectral range (*16*).

Device fabrication

First, a 3-μm-thick SiO_2 layer was deposited via plasma-enhanced chemical vapor deposition (PECVD) on p-type 8-inch silicon wafers to serve as the under-cladding oxide. Next, low-pressure chemical vapor deposition (LPCVD) was used to deposit a 750-nm silicon nitride

for the spiral resonators, with a gas mixture of SiH_2Cl_2 and NH_3. The resulting silicon nitride layer was patterned by optimized 248-nm deep ultraviolet lithography and etched down to the buried SiO_2 via optimized reactive ion dry etching. The sidewalls were observed under a scanning electron microscope with an etch verticality of 82° to 88° (see section SI). Then, the silicon nitride spiral resonators were annealed at 1200°C to reduce the N-H overtones absorption at the shorter wavelengths. Finally, the silicon nitride spiral resonators were overcladded with a 3-μm-thick SiO_2 layer, deposited initially with LPCVD (500 nm) and then with PECVD (2500 nm). The propagation loss of the Si_3N_4 waveguide was ~0.2 dB/cm at the pump wavelength.

SUPPLEMENTARY MATERIALS

Supplementary material for this article is available at http://advances.sciencemag.org/cgi/content/full/2/4/e1501489/DC1

I. Properties of the Si_3N_4 microresonator.
II. Low-noise state of the Kerr frequency comb.
III. Confirmation of the continuously equidistant Kerr frequency comb.
IV. Dependence of comb spacing on pump properties.
V. After-resonator feedback stabilization scheme and measurements.
fig. S1. Properties of the Si_3N_4 microresonator.
fig. S2. RF amplitude noise spectra of the high-noise state and the low-noise phase-locked comb state.
fig. S3. Confirmation of the continuously equidistant Kerr frequency comb.
fig. S4. Dependence of comb spacing on pump properties.
fig. S5. Schematic of the alternative experimental setup for the generation and stabilization of the chip-scale optical frequency comb.
References (*38*–*41*)

REFERENCES AND NOTES

1. D. K. Armani, T. J. Kippenberg, S. M. Spillane, K. J. Vahala, Ultra-high-*Q* toroid microcavity on a chip. *Nature* **421**, 925–928 (2003).
2. S. M. Spillane, T. J. Kippenberg, K. J. Vahala, K. W. Goh, E. Wilcut, H. J. Kimble, Ultrahigh-*Q* toroidal microresonators for cavity quantum electrodynamics. *Phys. Rev. A* **71**, 013817 (2005).
3. B. Peng, Ş. K. Özdemir, F. Lei, F. Monifi, M. Gianfreda, G. L. Long, S. Fan, F. Nori, C. M. Bender, L. Yang, Nonreciprocal light transmission in parity-time-symmetric whispering-gallery microcavities. *Nat. Phys.* **10**, 394–398 (2014).
4. M. R. Foreman, J. D. Swaim, F. Vollmer, Whispering gallery mode sensors. *Adv. Opt. Photonics* **7**, 168–240 (2015).
5. D. J. Moss, R. Morandotti, A. L. Gaeta, M. Lipson, New CMOS-compatible platforms based on silicon nitride and Hydex for nonlinear optics. *Nat. Photonics* **7**, 597–607 (2013).
6. A. Coillet, J. Dudley, G. Genty, L. Larger, Y. K. Chembo, Optical rogue waves in whispering-gallery-mode resonators. *Phys. Rev. A* **89**, 013835 (2014).
7. T. J. Kippenberg, R. Holzwarth, S. A. Diddams, Microresonator-based optical frequency combs. *Science* **332**, 555–559 (2011).
8. T. Herr, V. Brasch, J. D. Jost, C. Y. Wang, N. M. Kondratiev, M. L. Gorodetsky, T. J. Kippenberg, Temporal solitons in optical microresonators. *Nat. Photonics* **8**, 145–152 (2014).
9. S.-W. Huang, H. Zhou, J. Yang, J. F. McMillan, A. Matsko, M. Yu, D.-L. Kwong, L. Maleki, C. W. Wong, Mode-locked ultrashort pulse generation from on-chip normal dispersion microresonators. *Phys. Rev. Lett.* **114**, 053901 (2015).
10. X. Xue, Y. Xuan, Y. Liu, P.-H. Wang, S. Chen, J. Wang, D. E. Leaird, M. Qi, A. M. Weiner, Mode-locked dark pulse Kerr combs in normal-dispersion microresonators. *Nat. Photonics* **9**, 594–600 (2015).
11. V. Brasch, M. Geiselmann, T. Herr, G. Lihachev, M. H. P. Pfeiffer, M. L. Gorodetsky, T. J. Kippenberg, Photonic chip–based optical frequency comb using soliton Cherenkov radiation. *Science* **351**, 357–360 (2016).
12. P. Del'Haye, A. Schliesser, O. Arcizet, T. Wilken, R. Holzwarth, T. J. Kippenberg, Optical frequency comb generation from a monolithic microresonator. *Nature* **450**, 1214–1217 (2007).
13. M. A. Foster, J. S. Levy, O. Kuzucu, K. Saha, M. Lipson, A. L. Gaeta, Silicon-based monolithic optical frequency comb source. *Opt. Express* **19**, 14233–14239 (2011).
14. P. Del'Haye, O. Arcizet, A. Schliesser, R. Holzwarth, T. J. Kippenberg, Full stabilization of a microresonator-based optical frequency comb. *Phys. Rev. Lett.* **101**, 053903 (2008).
15. J. D. Jost, T. Herr, C. Lecaplain, V. Brasch, M. H. P. Pfeiffer, T. J. Kippenberg, Counting the cycles of light using a self-referenced optical microresonator. *Optica* **2**, 706–711 (2015).
16. J. Li, H. Lee, T. Chen, K. J. Vahala, Low-pump-power, low-phase-noise, and microwave to millimeter-wave repetition rate operation in microcombs. *Phys. Rev. Lett.* **109**, 233901 (2012).
17. A. A. Savchenkov, D. Eliyahu, W. Liang, V. S. Ilchenko, J. Byrd, A. B. Matsko, D. Seidel, L. Maleki, Stabilization of a Kerr frequency comb oscillator. *Opt. Lett.* **38**, 2636–2639 (2013).
18. S. B. Papp, P. Del'Haye, S. A. Diddams, Mechanical control of a microrod-resonator optical frequency comb. *Phys. Rev. X* **3**, 031003 (2013).
19. P. Del'Haye, K. Beha, S. B. Papp, S. A. Diddams, Self-injection locking and phase-locked states in microresonator-based optical frequency combs. *Phys. Rev. Lett.* **112**, 043905 (2014).
20. A. R. Johnson, Y. Okawachi, J. S. Levy, J. Cardenas, K. Saha, M. Lipson, A. L. Gaeta, Chip-based frequency combs with sub-100 GHz repetition rates. *Opt. Lett.* **37**, 875–877 (2012).
21. J. Pfeifle, V. Brasch, M. Lauermann, Y. Yu, D. Wegner, T. Herr, K. Hartinger, P. Schindler, J. Li, D. Hillerkuss, R. Schmogrow, C. Weimann, R. Holzwarth, W. Freude, J. Leuthold, T. J. Kippenberg, C. Koos, Coherent terabit communications with microresonator Kerr frequency combs. *Nat. Photonics* **8**, 375–380 (2014).
22. S.-W. Huang, J. Yang, J. Lim, H. Zhou, M. Yu, D.-L. Kwong, C. W. Wong, A low-phase-noise 18 GHz Kerr frequency microcomb phase-locked over 65 THz. *Sci. Rep.* **5**, 13355 (2015).
23. T. Ideguchi, S. Holzner, B. Bernhardt, G. Guelachvili, N. Picqué, T. W. Hänsch, Coherent Raman spectro-imaging with laser frequency combs. *Nature* **502**, 355–358 (2013).
24. S. A. Diddams, T. Udem, J. C. Bergquist, E. A. Curtis, R. E. Drullinger, L. Hollberg, W. M. Itano, W. D. Lee, C. W. Oates, K. R. Vogel, D. J. Wineland, An optical clock based on a single trapped $^{199}Hg^+$ ion. *Science* **293**, 825–828 (2001).
25. T. Udem, R. Holzwarth, T. W. Hänsch, Optical frequency metrology. *Nature* **416**, 233–237 (2002).
26. D. Hillerkuss, R. Schmogrow, T. Schellinger, M. Jordan, M. Winter, G. Huber, T. Vallaitis, R. Bonk, P. Kleinow, F. Frey, M. Roeger, S. Koenig, A. Ludwig, A. Marculescu, J. Li, M. Hoh, M. Dreschmann, J. Meyer, S. B. Ezra, N. Narkiss, B. Nebendahl, F. Parmigiani, P. Petropoulos, B. Resan, A. Oehler, K. Weingarten, T. Ellermeyer, J. Lutz, M. Moeller, M. Huebner, J. Becker, C. Koos, W. Freude, J. Leuthold, 26 Tbit s^{-1} line-rate super-channel transmission utilizing all-optical fast Fourier transform processing. *Nat. Photonics* **5**, 364–371 (2011).
27. S. T. Cundiff, A. M. Weiner, Optical arbitrary waveform generation. *Nat. Photonics* **4**, 760–766 (2010).
28. C.-H. Li, A. J. Benedick, P. Fendel, A. G. Glenday, F. X. Kärtner, D. F. Phillips, D. Sasselov, A. Szentgyorgyi, R. L. Walsworth, A laser frequency comb that enables radial velocity measurements with a precision of 1 cm s^{-1}. *Nature* **452**, 610–612 (2008).
29. T. Wilken, G. L. Curto, R. A. Probst, T. Steinmetz, A. Manescau, L. Pasquini, J. I. González Hernández, R. Rebolo, T. W. Hänsch, T. Udem, R. Holzwarth, A spectrograph for exoplanet observations calibrated at the centimetre-per-second level. *Nature* **485**, 611–614 (2012).
30. A. G. Glenday, C.-H. Li, N. Langellier, G. Chang, L.-J. Chen, G. Furesz, A. A. Zibrov, F. Kärtner, D. F. Phillips, D. Sasselov, A. Szentgyorgyi, R. L. Walsworth, Operation of a broadband visible-wavelength astro-comb with a high-resolution astrophysical spectrograph. *Optica* **2**, 250–254 (2015).
31. T. Herr, K. Hartinger, J. Riemensberger, C. Y. Wang, E. Gavartin, R. Holzwarth, M. L. Gorodetsky, T. J. Kippenberg, Universal formation dynamics and noise of Kerr-frequency combs in microresonators. *Nat. Photonics* **6**, 480–487 (2012).
32. S. B. Papp, P. Del'Haye, S. A. Diddams, Parametric seeding of a microresonator optical frequency comb. *Opt. Express* **21**, 17615–17624 (2013).
33. J. Ye, S. Swartz, P. Jungner, J. L. Hall, Hyperfine structure and absolute frequency of the ^{87}Rb $5P_{3/2}$ state. *Opt. Lett.* **21**, 1280–1282 (1996).
34. A. Bruner, V. Mahal, I. Kiryuschev, A. Arie, M. A. Arbore, M. M. Fejer, Frequency stability at the kilohertz level of a rubidium-locked diode laser at 192.114 THz. *Appl. Opt.* **37**, 6410–6414 (1998).
35. A. Arbabi, L. L. Goddard, Measurements of the refractive indices and thermo-optic coefficients of Si_3N_4 and SiO_x using microring resonances. *Opt. Lett.* **38**, 3878–3881 (2013).
36. A. B. Matsko, L. Maleki, On timing jitter of mode locked Kerr frequency combs. *Opt. Express* **21**, 28862–28876 (2013).
37. E. Rubiola, On the measurement of frequency and of its sample variance with high-resolution counters. *Rev. Sci. Instrum.* **76**, 054703 (2005).
38. A. A. Savchenkov, A. B. Matsko, W. Liang, V. S. Ilchenko, D. Seidel, L. Maleki, Kerr frequency comb generation in overmoded resonators. *Opt. Express* **20**, 27290–27298 (2012).

39. I. S. Grudinin, L. Baumgartel, N. Yu, Impact of cavity spectrum on span in microresonator frequency combs. *Opt. Express* **21**, 26929–26935 (2013).
40. Y. Liu, Y. Xuan, X. Xue, P.-H. Wang, S. Chen, A. J. Metcalf, J. Wang, D. E. Leaird, M. Qi, A. M. Weiner, Investigation of mode coupling in normal-dispersion silicon nitride microresonators for Kerr frequency comb generation. *Optica* **1**, 137–144 (2014).
41. S. B. Papp, K. Beha, P. Del'Haye, F. Quinlan, H. Lee, K. J. Vahala, S. A. Diddams, Microresonator frequency comb optical clock. *Optica* **1**, 10–14 (2014).

Acknowledgments: We acknowledge discussions with M. McDonald, H. Zhou, J. Lim, and A. Kumar Vinod. We also acknowledge J. G. F. Flores and Y. Huang for their assistance with the cross-sectional scanning electron micrographs and the loan of the microwave signal generator from the Bergman group at Columbia University. **Funding:** The authors acknowledge funding support from the Defense Advanced Research Projects Agency (HR0011-15-2-0014), the National Institute of Standards and Technology Precision Measurement Grant (60NANB13D163 to T.Z. and B.H.M.), the National Science Foundation (PHY-1349725 to T.Z. and B.H.M.), the Office of Naval Research (N00014-14-1-0041), and the Air Force Office of Scientific Research Young Investigator Award (FA9550-15-1-0081 to S.-W.H.).

Author contributions: S.-W.H. designed the measurements, analyzed the data, and wrote the paper. S.-W.H. and J.Y. performed the measurements. S.-W.H., J.Y., and C.W.W. designed the layout. M.Y. and D.-L.K. performed the device nanofabrication. B.H.M. and T.Z. aided in the measurements performed with the Menlo Systems FFC. All authors contributed to the discussion and revision of the manuscript. **Competing interests:** The authors declare that they have no competing interests. **Data and materials availability:** All data needed to evaluate the conclusions in the paper are present in the paper and/or the Supplementary Materials. Additional data related to this paper may be requested from the authors.

Submitted 20 October 2015
Accepted 17 March 2016
Published 22 April 2016
10.1126/sciadv.1501489

Citation: S.-W. Huang, J. Yang, M. Yu, B. H. McGuyer, D.-L. Kwong, T. Zelevinsky, C. W. Wong, A broadband chip-scale optical frequency synthesizer at 2.7×10^{-16} relative uncertainty. *Sci. Adv.* **2**, e1501489 (2016).

Science Advances

AAAS

advances.sciencemag.org/cgi/content/full/2/4/e1501489/DC1

Supplementary Materials for

A broadband chip-scale optical frequency synthesizer at 2.7×10^{-16} relative uncertainty

Shu-Wei Huang, Jinghui Yang, Mingbin Yu, Bart H. McGuyer, Dim-Lee Kwong, Tanya Zelevinsky, Chee Wei Wong

Published 22 April 2016, *Sci. Adv.* **2**, e1501489 (2016)
DOI: 10.1126/sciadv.1501489

The PDF file includes:

I. Properties of the Si_3N_4 microresonator

Figure S1A shows a cross-section scanning electron micrograph of the microresonator waveguide, with an estimated 82° to 88° slope of the vertical sidewalls. The refractive index of the low pressure chemical vapor deposition (LPCVD) Si_3N_4 film was measured with an ellipsometric spectroscopy (Woollam M-2000 ellipsometer) and then fitted with the Sellmeier equation assuming a single absorption resonance in the ultraviolet. The fitted Sellmeier equation, $n(\lambda) = \sqrt{1 + \frac{2.90665\lambda^2}{\lambda^2 - 145.05007^2}}$, and the sidewall angle were both imported into the COMSOL Multiphysics for the microresonator design. Figure S1B shows the modeled free spectral range (FSR) of the first two TE modes of the microresonator. While the fundamental mode features a FSR of 17.9 GHz, the TE_2 mode has a slightly lower FSR and thus the resonances of the TE_2 family approaches that of the fundamental family about every 4 nm ($\frac{FSR^2}{\Delta FSR} = 460GHz$). The mode interaction when the resonances are close leads to local disruption of the phase matching condition *(37-39)* and results in the periodic amplitude modulation on the Kerr comb spectrum (Fig. 1B).

Figures S1C and S1D show the modeled group velocity dispersion (β_2, GVD) and third order dispersion (β_3, TOD). The non-equidistance of the cold cavity modes, $D = (\omega_{m+1} - \omega_m) - (\omega_m - \omega_{m-1})$, can be calculated using the equation $D = -\frac{(\beta_2 L)}{2\pi}\omega_{FSR}^3 + \frac{(\beta_2 L)^2}{4\pi^2}\omega_{FSR}^5 - \frac{(\beta_3 L)}{4\pi}\omega_{FSR}^4$, where L is the cavity's length and ω_{FSR} is the cavity's free spectral range.

Due to the large refractive index of the Si_3N_4 waveguide, a 600 μm long adiabatic mode converter (the Si_3N_4 waveguide, embedded in the 5×5 μm^2 SiO_2 waveguide, has gradually changing widths from 0.2 μm to 1 μm) is implemented to improve the coupling efficiency from the free space to the bus waveguide. The input-output insertion loss for the waveguide does not exceed 6 dB.

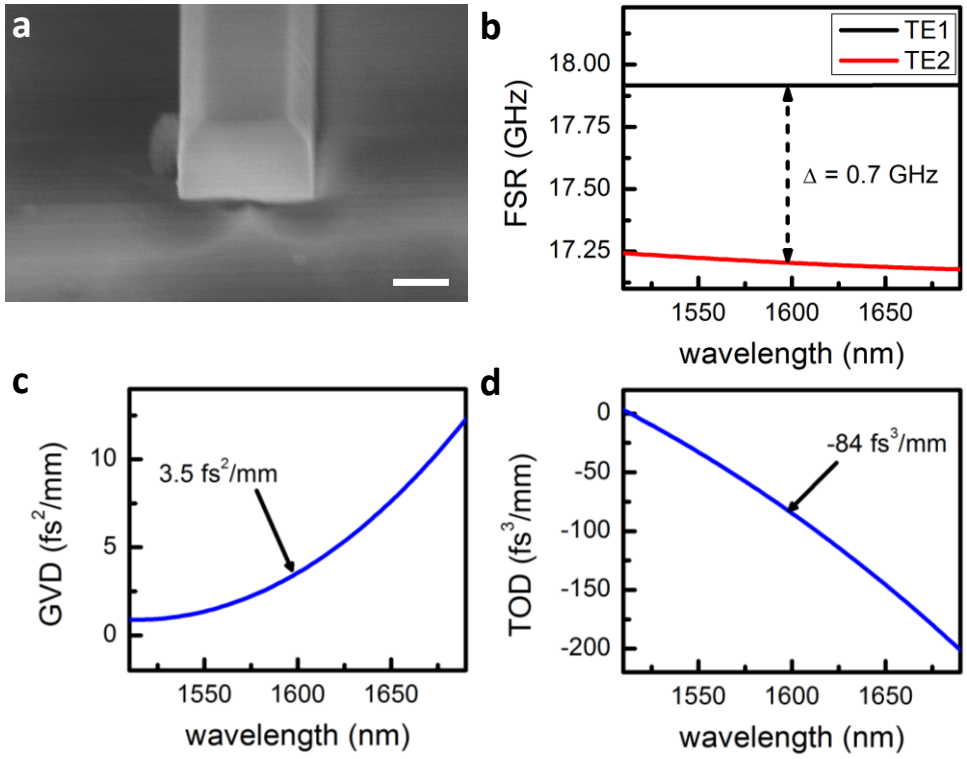

fig. S1. Properties of the Si_3N_4 microresonator. (a) Scanning electron micrograph of the waveguide cross-section. Scale bar: 500 nm. **(b)** Modeled free spectral range of the first two TE modes of the chip-scale optical frequency comb. **(c)** Modeled group velocity dispersion of the fundamental mode, measuring a GVD of 3.5 fs^2/mm at the pump wavelength. **(d)** Modeled third order dispersion of the fundamental mode, measuring a TOD of -84 fs^2/mm at the pump wavelength.

II. Low-noise state of the Kerr frequency comb

As the pump wavelength was tuned into the resonance from the high frequency side, we first observed multiple RF spikes because the primary comb line spacing is incommensurate with the fundamental comb spacing. The state with incommensurate spacing was unstable and it made frequent transition to high-noise state characterized by elevated RF amplitude noise (45 dB higher than the phase-locked comb state). Next, with fine control of the pump wavelength (10 MHz/step), the offset between different comb families can be made zero such that the RF amplitude noise spectrum showed no excess noise (fig. S2). The phase-locked comb typically stabilized for hours.

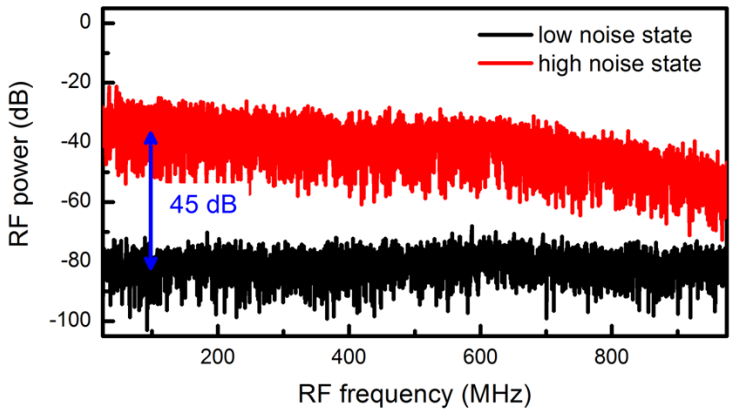

fig. S2. RF amplitude noise spectra of the high-noise state and the low-noise phase-locked comb state. With the proper pump wavelength, RF amplitude noise dropped by 45 dB and approached the detector background noise, indicative of the transition into a phase-locked state.

III. Confirmation of continuously equidistant Kerr frequency comb

To verify the Kerr frequency comb is continuously equidistant, not consisted of many sub-comb families with offsets *(30)*, we measured the comb spacing and the amplitude noise of various different filtered segments of the Kerr frequency comb (1553.5-1554.5nm, 1555-1556nm, 1556.2-1557.2nm, 1558-1559nm, 1560-1561nm, 1561.7-1562.7nm, 1563.5-1564.5nm, 1566-1567nm, 1568.5-1569.5nm, 1570.5-1571.5nm, 1572.3-1573.3nm, 1574-1575nm, 1577-1578nm 1578.5-1579.5nm, 1580.3-1581.3nm). The comb spacing was measured to be identical at 17.9 GHz within the RBW of 390 kHz (fig. S3A) and 1 kHz (fig. S3B) for the 15 filtered comb segments from 1553.5nm to 1581.3nm. No other peaks were observed. Absence of sub-comb families with offset frequencies was also independently confirmed by the amplitude noise measurements, showing no peaks and excess noise above the detector background noise. The Kerr microcomb's continuous equidistance was thus verified.

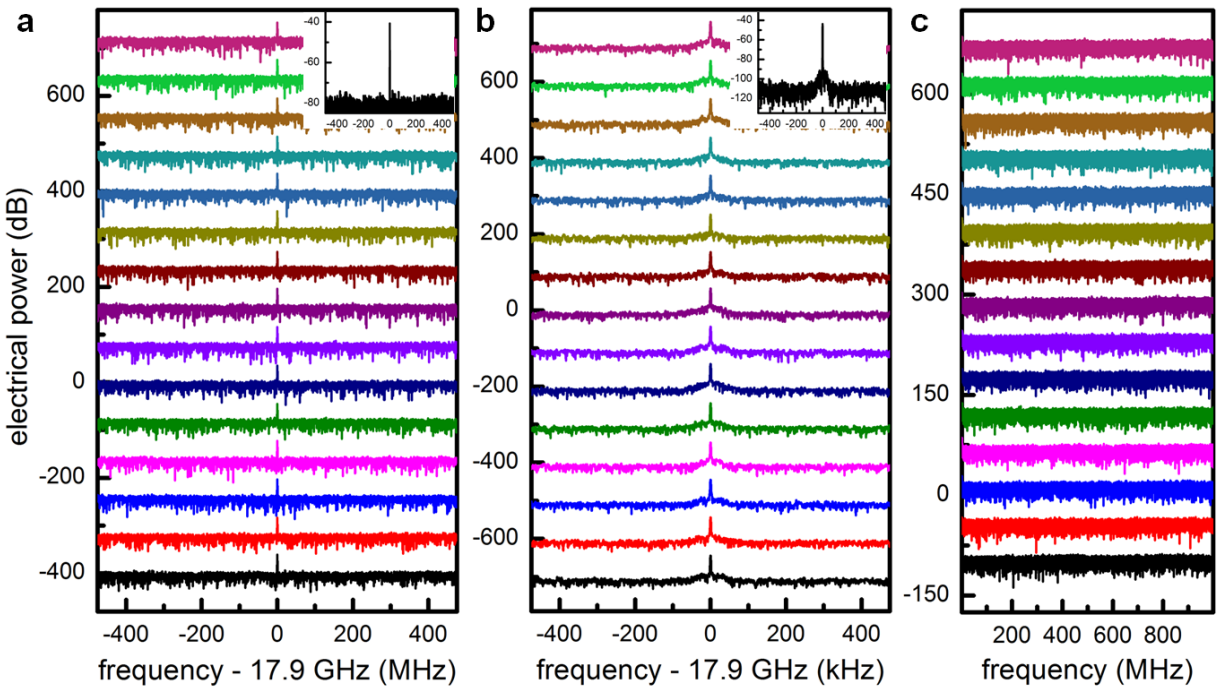

fig. S3. Confirmation of the continuously equidistant Kerr frequency comb. (a) Comb spacing spectra of 15 filtered comb segments with scan ranges of 1 GHz. **(b)** Comb spacing spectra of 15 filtered comb segments with scan ranges of 1 MHz. **(c)** Amplitude noise spectra of 15 filtered comb segments with a scan range of 1 GHz.

IV. Dependence of comb spacing on pump properties

After the Kerr frequency comb was driven into the low phase noise state, we characterized the dependence of the comb spacing on the pump properties by adding a 0.1 Hz sinusoidal change of either pump frequency or pump power and measuring the corresponding comb spacing oscillation amplitude with a frequency counter.

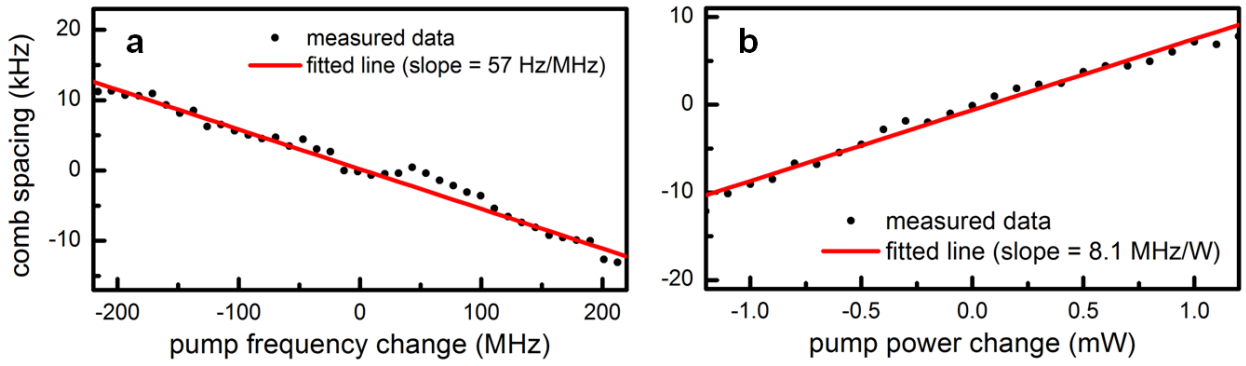

fig. S4. Dependence of comb spacing on pump properties. (a) The comb spacing as a function of the pump frequency change, determined at 57 Hz/MHz in our microresonator. **(b)** The comb spacing as a function of the pump power change in the ring, determined at 8.1 MHz/W in our microresonator.

V. After-resonator feedback stabilization scheme and measurements

As discussed in the main text, a rubidium locked diode laser at 1560 nm can also be used as the optical reference for phase locking one of the comb lines (*16, 33, 40*). As Si_3N_4 microresonators suffer from lower *Q* at optical C-band due to residual N-H absorption *(9)*, we prefer to pump the microresonator at optical L-band for low threshold comb generation. In the alternative scheme, the 1560 nm comb line is thus only accessible after the microresonator when the Kerr microcomb is generated (fig. S5). Here the 1560 nm comb line was selected by a narrowband monochromator and beat with the optical reference on a photodetector after the comb generation stage. The rest of the setup was the same as the one shown in Fig. 1A. Figure S5B shows that the beat note can be equally well stabilized to a resolution limited linewidth of 6 Hz.

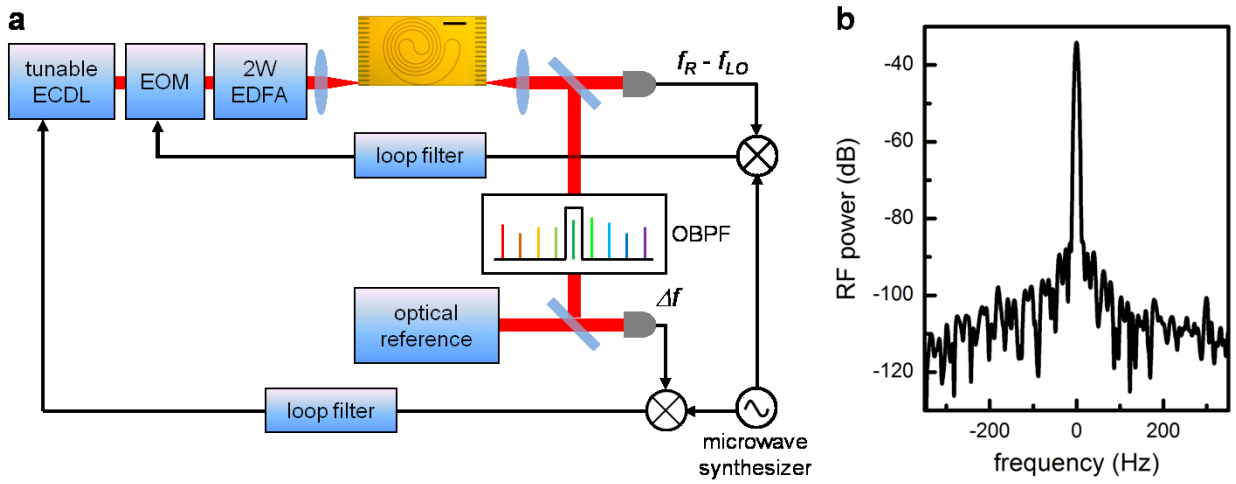

fig. S5. Schematic of the alternative experimental setup for the generation and stabilization of the chip-scale optical frequency comb. (a) After the microresonator, the 1560 nm comb line was selected by a narrowband monochromator and beat with the optical reference on a photodetector. The rest of the setup was the same as the one shown in Fig. 1A. **(b)** RF spectrum of the stabilized beat note, showing a resolution limited linewidth of 6 Hz. Control of the comb line frequency was achieved by modulating the diode current of the ECDL. OBPF: optical bandpass filter.